Telecom-Wavelength Atomic Quantum Memory in Optical Fiber for Heralded Polarization Qubits

Jeongwan Jin, Erhan Saglamyurek, Marcel. lí Grimau Puigibert, Varun Verma, Francesco Marsili, Sae Woo Nam, Daniel Oblak, and Wolfgang Tittel

Phys. Rev. Lett. **115**, 140501 — Published 28 September 2015

DOI: 10.1103/PhysRevLett.115.140501

A telecom-wavelength atomic quantum memory in optical fiber for heralded polarization qubits

Jeongwan Jin,[1,*] Erhan Saglamyurek,[1] Marcel.lí Grimau Puigibert,[1] Varun Verma,[2] Francesco Marsili,[3] Sae Woo Nam,[2] Daniel Oblak,[1] and Wolfgang Tittel[1,†]

[1] *Institute for Quantum Science and Technology, and Department of Physics & Astronomy, University of Calgary, 2500 University Drive NW, Calgary, Alberta T2N 1N4, Canada*
[2] *National Institute of Standards and Technology, Boulder, Colorado 80305, USA*
[3] *Jet Propulsion Laboratory, California Institute of Technology, 4800 Oak Grove Drive, Pasadena, California 91109, USA*

Polarization-encoded photons at telecommunication wavelengths provide a compelling platform for practical realizations of photonic quantum information technologies due to the ease of performing single qubit manipulations, the availability of polarization-entangled photon-pair sources, and the possibility of leveraging existing fiber-optic links for distributing qubits over long distances. An optical quantum memory compatible with this platform could serve as a building block for these technologies. Here we present the first experimental demonstration of an atomic quantum memory that directly allows for reversible mapping of quantum states encoded in the polarization degree of a telecom-wavelength photon. We show that heralded polarization qubits at a telecom-wavelength are stored and retrieved with near-unity fidelity by implementing the atomic frequency comb protocol in an ensemble of erbium atoms doped into an optical fiber. Despite remaining limitations in our proof-of-principle demonstration such as small storage efficiency and storage time, our broadband light-matter interface reveals the potential for use in future quantum information processing.

PACS numbers:

Photon-based quantum information processing promises new technologies including optical quantum computing, quantum cryptography, and distributed quantum networks. The realization of these technologies rely on encoding quantum information (e.g. qubits) into single photons, and processing and distributing it to distant locations. In principle, a qubit can be encoded into any photonic degree of freedom, but the polarization degree has often been a preferred choice due to the ease of performing single qubit manipulations and projection measurements using wave-plates and polarizing beam-splitters, and the availability of polarization-entangled photon-pair sources [1]. On this background many seminal demonstrations of quantum information processing have employed polarization qubits, such as teleportation [2], entanglement swapping [3], and secure quantum key distribution over more than hundred kilometers [4], pointing towards the possibility to build secure quantum networks [5].

In addition to polarization encoding, the realization of future quantum networks will be greatly facilitated by the use of existing fiber optic infrastructure, which allows low propagation loss for photons at wavelengths around 1550 nm, commonly referred to as telecom-wavelengths [6]. Nevertheless, propagation loss still limits the distance of such quantum links to a few hundreds kilometers. This distance barrier may be overcome by the development of quantum repeaters [7]. These, in turn, rely on the ability to store photonic qubits in quantum memories to overcome the probabilistic nature of photon transmission through lossy quantum channels and emission from currently used single-photon sources [8, 9]. However, to date, no quantum memory for polarization qubits encoded into telecom wavelength photons has been demonstrated. In fact, until recently [18], direct quantum storage of telecom-wavelength photons was an unsolved problem. The most promising candidate, erbium, has the required transition wavelength but exhibits atomic-level dynamics that have shown to be challenging for non-classical light storage [10, 11]. This has prompted indirect approaches such as quantum state teleportation [12] or coherent conversion techniques [13] from telecom-wavelength photons to photons at other wavelengths at which existing quantum memories can operate.

Furthermore, storage of polarization qubits at any wavelength is inhibited by the fact that the interaction of polarized light with most atomic media has orientational dependence, and birefringence in solid state materials often complicates matters further. In a few experiments – using light outside the telecom range – this has been circumvented by storing each polarization component in two spatially separated parts of a memory that each only interact with a single polarization component [14–17]. However, this begs the question if there exists a solid-state material in which absorbers in an ensemble are aligned uniformly so that, in essence, all polarizations of light are equally coupled. Recent advances in the development of quantum memories based on erbium doped glass fiber point exactly in this direction [18]. Because glass constitutes an amorphous host, the transition dipole moment of embedded rare-earth ions has no preferred direction, resulting in uniform coupling of an ensemble to all light polarizations. Moreover, the possibility to splice fiber-based memories with standard telecommunication

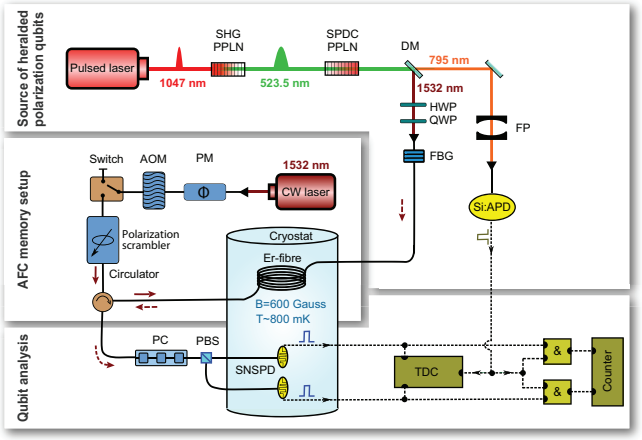

FIG. 1: Experimental setup: In the heralded polarization qubit source, 6 ps long, 80 MHz repetition-rate pulses at 1047 nm wavelength are frequency doubled and subsequently downconverted in periodically poled lithium niobate crystals (PPLN). This generates photon pairs at 795 nm and 1532 nm (telecom) wavelengths, which are spectrally filtered with a Fabry-Perot (FP) cavity and a Fiber-Bragg grating (FBG), respectively. Detection of the 795 nm photon by a Si-APD (60% detection efficiency and 600 ps timing-jitter) heralds the presence of the telecom photon, and a half-wave-plate (HWP) and quarter-wave-plate (QWP) prepare it in any desired polarization qubit state. The quantum memory consists of a 20-meter-long erbium doped fiber exposed to a 600 G magnetic field and cooled to 0.8 K using a cryostat. The polarization-insensitive AFC is prepared by optical pumping with continuous wave (CW) laser light at 1532 nm, which is frequency and amplitude modulated by phase modulator (PM) and an acousto-optic modulator (AOM), respectively, and polarization-randomized by a polarization scrambler with 5 KHz cycling frequency. For the qubit analysis, the recalled photons pass through a fiber-optic polarization controller (PC) and polarizing beam splitter (PBS) after which they impinge on one of two superconducting nano-wire single photon detectors (SNSPD) held at 0.8 K (60% system efficiency and 350 ps time-jitter). A set of AND gates counts coincidences between the qubit detection signals and the heralding signal, and a time-to-digital (TDC) converter additionally provides time mapping of the single detections of the 1532 nm photons compared to the moment of detection of the heralding photons at 795 nm wavelength.

fibers promises simple and low-loss integration with other components in a network.

In this letter, we report the faithful storage of polarization states of heralded telecom-wavelength single-photons in collective excitation of an atomic ensemble by implementing the atomic frequency comb (AFC) protocol in a cryogenically cooled erbium-doped optical fiber. We verify the memory's ability to store any polarization state with close to equal probability, and demonstrate its quantum nature by showing that recalled single photon polarization qubit states have a near unity fidelity with the originally prepared states.

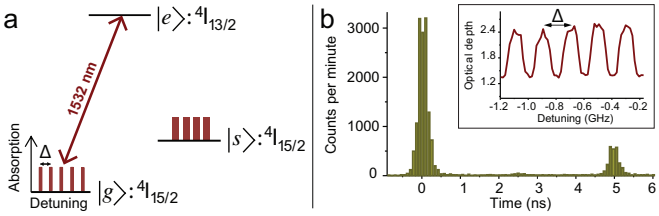

FIG. 2: (a) Simplified erbium level scheme: The AFC is prepared via frequency-selective population transfer from the $^4I_{15/2}$ electronic ground state ($|g\rangle$) through the $^4I_{13/2}$ excited state ($|e\rangle$) into an auxiliary (spin) state ($|s\rangle$). (b) Detection signal from a single SNSPD recorded by the TDC, showing directly transmitted and stored photons spaced by 5 ns. The inset shows a 1 GHz wide section of a typical AFC of 8 GHz total bandwidth. The background absorption arises from imperfect optical pumping.

Our experimental setup, sketched in Fig 1, is composed of three main parts: A fiber-based atomic quantum memory, a source of heralded polarization qubits, and a qubit analyzer. In the first step (middle panel of Fig. 1) we prepare the AFC memory using an optical pumping beam from a continuous wave laser. The beam is frequency and amplitude modulated before entering a 20 meter-long erbium-doped fiber cooled to 0.8 K with a cryostat based on a pulse-tube cooler and an adiabatic demagnetization refrigerator. The spectral profile of the pump light is chosen to be a square modulation with a period Δ. As indicated in Fig. 2a, this results in frequency-selective excitation of the erbium ions on their large inhomogeneously broadened transition line at 1532 nm. The polarization of the pump light can be actively scrambled to address erbium ions interacting with different polarization modes in the fiber. The scrambling is performed by a polarization controller that is programmed to randomly change the polarization of the light every 500 μs. We maintain the optical pumping for 500 ms, which leads to atoms with transition frequencies matching the pumping light to accumulate in a long lived electronic Zeeman level that arises under the application of a magnetic field of 600 Gauss. This process allows us to generate an 8 GHz broad comb-shaped absorption profile – that is an AFC – having a tooth spacing of $\Delta = 200$ MHz and finesse (ratio of peak spacing to width) of 2 (a 1 GHz broad section is shown in the inset of Fig. 2b). To avoid photons stemming from spontaneous decay of atoms in the excited state during qubit recall, a wait time of 300 ms is set after the optical pumping. During 700 ms, following the wait time, we can map a photon onto our AFC, giving rise to collective excitation of the erbium ions in what is commonly referred to as a Dicke state:

$$|\Psi\rangle = \frac{1}{\sqrt{N}} \sum_{j=1}^{N} c_j e^{i2\pi m_j \Delta t} e^{-ikz_j} |g_1, \cdots e_j, \cdots g_N\rangle \quad . \quad (1)$$

Here, $|g_j\rangle$ ($|e_j\rangle$) is the ground (excited) state of atom j, $m_j\Delta$ is the detuning of the transition frequency of the atom from the photon carrier frequency, z_j is the atom's position measured along the propagation direction of the light, and the factor c_j depends on the resonance frequency and position of the atom. Due to the different atomic transition frequencies, each excitation term in the Dicke state accumulates a different phase over time. However, the periodic structure of the transition frequencies of atomic absorbers in the AFC leads the phases to realign at a time given by the inverse of the peak spacing $t_{storage} = 1/\Delta$ [19]. Consequently, for Δ=200 MHz, an input photon is retrieved after $t_{storage} = 5$ ns in the originally encoded state, as shown in Fig. 2b.

The second step is to prepare heralded polarization qubits, that are compatible with our light-matter interface, using the photon pair source (top panel of Fig. 1). To this end, short pulses produced from a mode-locked laser operating at 1047 nm wavelength are frequency doubled via second harmonic generation (SHG). The resulting pulses at 523 nm are sent to a periodically-poled lithium niobate crystal where they take part in a spontaneous parametric down conversion (SPDC) process. The phase matching condition for SPDC results in a pair of photons at 1532 nm and 795 nm, named *signal* and *idler* photons, respectively. In order to match the acceptance bandwidth of our storage device, the bandwidths of the 1532 nm and 795 nm photons are filtered down to nearly 10 GHz. The 795 nm photons are then directly detected by a Si-APD single-photon detector to provide a heralding signal. The 1532 nm photons pass through a free-space Half-Wave Plate (HWP) and Quarter-Wave Plate, which allow us to encode the polarization states

$$|\psi\rangle = \cos\theta|H\rangle + e^{i\varphi}\sin\theta|V\rangle \ , \qquad (2)$$

where $|H\rangle$ and $|V\rangle$ denote a horizontally and vertically polarized 1532 nm photon, and $\cos\theta$ and $\sin\theta$ are the probability amplitudes for $|H\rangle$ and $|V\rangle$, respectively. At this point the prepared polarization qubits are sent to the prepared AFC memory for storage and recall.

The final step is to analyze the recalled qubits using the analyzer shown in the bottom panel of Fig. 1. Its optical part consists of a polarization controller followed by a polarizing beam-splitter (PBS) with super-conducting nanowire single-photon detectors (SNSPD) at each output. These allow making projection measurements onto any set of orthogonal polarization qubit states. The electronic part consists of logic gates that enable counting coincidences with the heralding signal.

In our measurements we first characterize the polarization sensitivity of our fiber-based atomic memory with and without the polarization scrambling of the optical pumping light. We gradually change the polarization state of the 1532 nm photons from horizontal to vertical by rotating the free-space HWP in steps of 15 degrees.

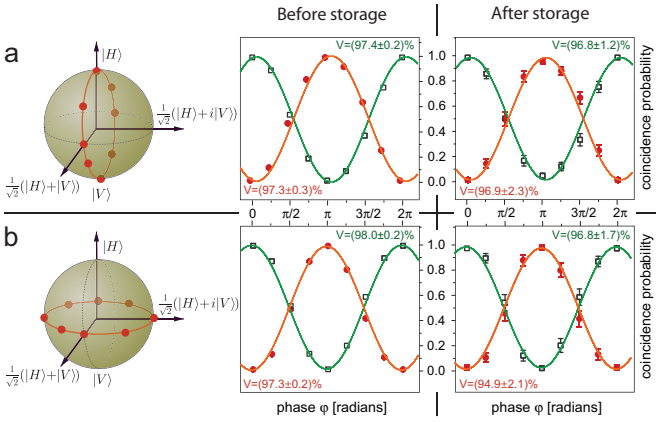

FIG. 3: Measured coincidence probabilities for detecting the heralding photon and the telecom-photon at either output of the PBS for qubit states of the form (a) $|\psi\rangle = \cos\theta|H\rangle + \sin\theta|V\rangle$ projected onto $|H\rangle$ (squares) and $|V\rangle$ (circles) and of the form (b) $|\psi\rangle = \frac{1}{\sqrt{2}}(|H\rangle + e^{i\varphi}|V\rangle$ projected onto $|+\rangle = \frac{1}{\sqrt{2}}(|H\rangle + |V\rangle$ (squares) and $|-\rangle = \frac{1}{\sqrt{2}}(|H\rangle - |V\rangle$ (circles). The left-hand-side and the right-hand-side are before and after storage in the AFC, respectively. Probabilities are calculated by dividing the coincidence counts at each PBS output during 5 minutes by the total coincidence counts (i.e. the sum of the counts in the two PBS outputs), which is approximately 1 Hz. Error-bars are based on Poissonian detection statistics and all visibility values are based on sine fits to the data.

For each polarization setting we store the 1532-nm photons in our AFC memory first without, and then with the polarization scrambler engaged. In this test, we disregard the heralding signal from the 795 nm photon detection and bypass the PBS such that we detect the retrieved 1532 nm photons using a single SNSPD, and normalize to the 5% polarization dependence of its detection efficiency [20].

Without the polarization scrambler we observe that the number of counts, and hence the efficiency of the memory, varies by about 25% with the polarization setting. This is due to the mismatch of the polarization state of the optical pumping light and the 1532 nm single photons, which counter-propagate through the fiber. This phenomenon is also known as "polarization hole-burning" in the operation of erbium-doped fiber amplifiers [21]. However, *with* polarization scrambling the generated AFC in any spatial section of the fiber consists of erbium ions that can be excited by arbitrary polarization state of the heralded single photons. In this case, the recall efficiency is near the maximum for all the utilized input polarization states. Remaining fluctuations of the overall AFC efficiency (up to 7%) are due to unstable operation of the optical pumping laser over the course of the measurements.

Next, in order to verify the quantum nature of the stor-

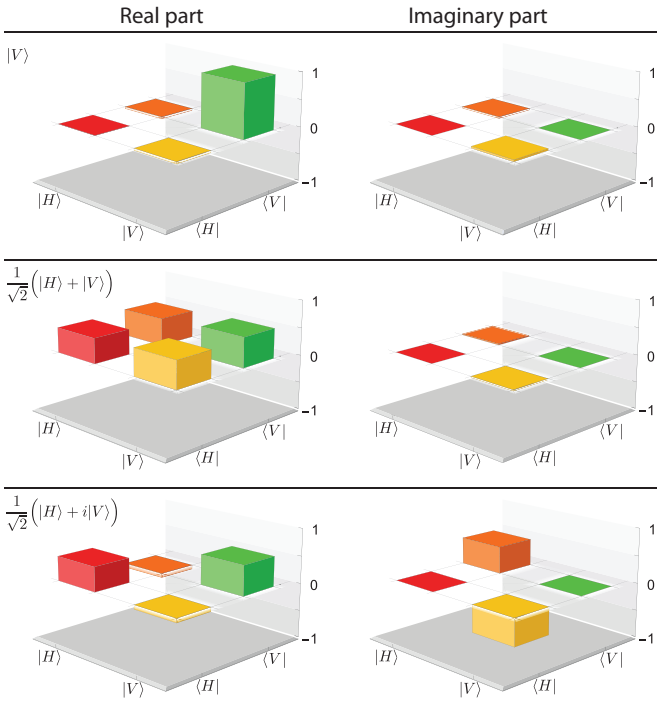

FIG. 4: Density matrices reconstructed from projection measurements of a set of input qubit states after storage of the heralded telecom photon. Fidelities with photons in ideal input states are indicated in Table I.

age we measure the second-order cross-correlation $g^{(2)}_{si}$

$$g^{(2)}_{si} = \frac{P_{si}}{P_i P_s} \ , \tag{3}$$

where P_{si} is the probability of coincidence detection between the heralding signal and the two qubit analyzer outputs combined. P_s and P_i are the detection probabilities for the 795 nm and the 1532 nm photons, respectively. Measuring a value $g^{(2)}_{si} > 2$ indicates the presence of quantum correlations between the photons in each pair, where we assume that the (non-heralded) auto-correlation values for the signal and idler photons are in between 1 and 2, corresponding to a coherent and a thermal state, respectively. We find $g^{(2)}_{si}$ to be 14.1 ± 0.3 before storage and, crucially, 18.4 ± 1.2 after storage, which demonstrates that quantum correlations between the members of the photon pairs are preserved during the storage. This also implies that the heralded auto-correlation function for the signal photon is $\ll 1$ [22], and hence we refer to the latter as a heralded single photon. The reason for $g^{(2)}_{si}$ to increase after storage is due to spectral filtering of the input photons (10 GHz bandwidth) caused by the slightly smaller bandwidth of the AFC memory (8 GHz), which results in a lower effective mean-photon number.

With this in hand, we now store of heralded polarization qubits. To begin, we either vary the phase θ to create the states $|\psi\rangle = \cos\theta|H\rangle + \sin\theta|V\rangle$ and set the qubit analyzer to project onto the states $|H\rangle$ and $|V\rangle$, or we vary φ to create the states $|\psi\rangle = (|H\rangle + e^{i\varphi}|V\rangle)/\sqrt{2}$ and set the qubit analyzer to project onto $(|H\rangle \pm |V\rangle)/\sqrt{2}$. In both cases, the projection rates are expected to vary sinusoidally with either θ or φ. To assess if our memory affects the stored qubits we perform the measurements both when the 1532 nm photons are recalled from the memory, and when they are just passing through the fiber, i.e. when the AFC is not activated. For each projection setting we monitor the outputs of the qubit analyzer over 5 minutes and count the detections of the 1532 nm photons that are in coincidence with the detections of the 795 nm photons (heralding signal) using an AND-gate. The data points and the resulting visibility curves in Fig. 3a-b show the variation of the coincidence probability for the two sets of input states as a function of the input polarization before and after storage. From the fitted visibilities we find the average fidelities $F_{H/V} = (2 + \mathcal{V}_H + \mathcal{V}_V)/4$ for projections onto $|H\rangle$ and $|V\rangle$ to be $(98.67 \pm 0.09)\%$ and $(98.4 \pm 0.6)\%$ before and after storage, respectively. Similarly for projections onto $(|H\rangle + e^{i\varphi}|V\rangle)/\sqrt{2}$ the fidelities are $(98.83 \pm 0.07)\%$ and $(97.93 \pm 0.7)\%$. These result show, within experimental uncertainty, that the qubit states have not been altered during storage.

Target qubit	Fidelity (%)	Target qubit	Fidelity (%)
$\|H\rangle$	99.7 ± 1.7	$\|V\rangle$	99.6 ± 3.0
$\frac{1}{\sqrt{2}}(\|H\rangle + \|V\rangle)$	99.6 ± 2.6	$\frac{1}{\sqrt{2}}(\|H\rangle - \|V\rangle)$	99.5 ± 2.6
$\frac{1}{\sqrt{2}}(\|H\rangle + i\|V\rangle)$	99.0 ± 5.0	$\frac{1}{\sqrt{2}}(\|H\rangle - i\|V\rangle)$	99.7 ± 1.8

TABLE I: Fidelities of reconstructed density matrices with target states.

To confirm this conclusion, we additionally perform quantum state tomography of several qubit states after recall from our AFC memory. In separate measurements we encode the states $|H\rangle$, $|V\rangle$, $(|H\rangle \pm |V\rangle)/\sqrt{2}$ and $(|H\rangle \pm i|V\rangle)/\sqrt{2}$, which form three mutually unbiased qubit bases, and map them to our memory. We retrieve the photons and, for each qubit, set the analyzers to project them onto the states $|H\rangle$ and $|V\rangle$, $(|H\rangle \pm |V\rangle)/\sqrt{2}$, and $(|H\rangle \pm i|V\rangle)/\sqrt{2}$. Using the outcomes of the coincidence measurements described previously, we reconstruct the quantum state of each retrieved qubit in terms of the density matrix [23] (See Fig. 4). All reconstructed density matrices have fidelities with the intended qubit states (listed in Table I) of 0.99 or above, which confirms that the memory preserves polarization qubit states. We associate the small difference of these fidelities from unity with imperfect state preparation and thus not as being due to the storage.

Despite these important results, the performance of our storage device needs to be improved for practical use in quantum photonic applications. First, the recall

efficiency is limited to ∼1% (for 5 ns storage), due to imperfect preparation of the AFC (see Fig. 2b). However, as discussed in detail in [18] and characterized in [24], the recall efficiency could be increased close to unity by improving the optical pumping dynamics using lower temperature and lower erbium concentrations and implementing the relevant phase matching conditions [19]. Second, the storage time in our current implementation is limited to 50 ns. This is mainly due to optical coherence time being affected by coupling of erbium ions to two-level systems, which are intrinsic in glass-like disordered hosts, as well as magnetic interactions between the erbium ions. Although the coherence time in lightly doped erbium fibers, such as ours, is expected to exceed 5 μs at temperatures approaching 100 mK, it remains a challenge to achieve the storage times required for quantum repeaters.

Yet, even with short storage times our light-matter interface possesses a number of features – such as a large time-bandwidth product, multimode storage capacity, and ability to process qubits – that makes it a good candidate for realizing on-demand single-photon sources [25] or programmable atomic processors [26]. In addition, erbium-based memories may be employed as quantum interfaces between telecommunication photons and superconducting circuits [27].

Finally, we note that our implementation provides a pre-programmed delay given by the inverse of the AFC peak spacing. Yet, spectrally-multiplexed storage with fixed storage time supplemented by feed-forward controlled recall is sufficient to implement quantum communication schemes [28].

In conclusion, we have realized quantum storage of polarization states encoded into heralded telecom-wavelength photons by implementing the AFC protocol in an erbium-doped optical fiber. Despite current limitations in terms of storage time and efficiency, the large bandwidth and multimode capacity of our light-matter interface are ideally suited for various applications in a future quantum Internet, e.g. for linear optics quantum computing and photonic quantum state processing. Furthermore, the robust and simple fiber-based platform of our light-matter interface offers full compatibility with quantum photonics relying on telecom-fiber technology.

We thank Raju Valivarthi, Qiang Zhou, Matthew D. Shaw and Vladimir Kiselyov for useful discussions and technical support, and gratefully acknowledge support through Alberta Innovates Technology Futures (AITF) and the National Science and Engineering Research Council of Canada (NSERC). W.T. is a senior fellow of the Canadian Institute for Advanced Research (CIFAR). VBV and SWN acknowledge partial funding for detector development from the Defense Advanced Research Projects Agency (DARPA) Information in a Photon (InPho) program. Part of the research was carried out at the Jet Propulsion Laboratory, California Institute of Technology, under a contract with the National Aeronautics and Space Administration.

J.J. and E.S. contributed equally to this work.

References

* Present address: Institute for Quantum Computing, Department of Physics and Astronomy, University of Waterloo, 200 University Ave West, Waterloo, Ontario, Canada
† Electronic address: wtittel@ucalgary.ca

[1] P. G. Kwiat, K. Mattle, H. Weinfurter, A. Zeilinger, A. V. Sergienko, and Y. Shih. *Phys. Rev. Lett.*, **75**, 4337–4341 (1995).
[2] D. Bouwmeester, J.-W. Pan, K. Mattle, M. Eibl, H. Weinfurter, and A. Zeilinger. *Nature*, **390**, 575–579 (1997).
[3] J.-W. Pan, D. Bouwmeester, H. Weinfurter, and A. Zeilinger. *Phys. Rev. Lett.*, **80**, 3891–3894 (1998).
[4] C.-Z. Peng, J. Zhang, D. Yang, W.-B. Gao, H.-X. Ma, H. Yin, H.-P. Zeng, T. Yang, X.-B. Wang, and J.-W. Pan. *Phys. Rev. Lett.*, **98**, 010505 (2007).
[5] N. Gisin, G. Ribordy, W. Tittel, and H. Zbinden. *Rev. Mod. Phys.*, **74**, 145–195 (2002).
[6] H. J. Kimble. *Nature*, **453**, 1023–1030 (2008).
[7] N. Sangouard, C. Simon, H. de Riedmatten, and N. Gisin. *Rev. Mod. Phys.*, **83**, 33–80 (2011).
[8] A. I. Lvovsky, B. C. Sanders, and W. Tittel. *Nature Photon.*, **3**, 706–714 (2009).
[9] F. Bussières, N. Sangouard, M. Afzelius, H. de Riedmatten, C. Simon, and W. Tittel. *J. Mod. Opt.*, **60**, 1519–1537 (2013).
[10] B. Lauritzen, J. Minář, H. de Riedmatten, M. Afzelius, N. Sangouard, C. Simon, and N. Gisin. *Phys. Rev. Lett.*, **104**, 080502 (2010).
[11] J. Dajczgewand, J. L. Le Gouët, A. Louchet-Chauvet, and T. Chanelière. *Opt. Lett.*, **39**, 2711–2714 (2014).
[12] F. Bussières *et al. Nature Photon.*, **8**, 775–778 (2014).
[13] N. Maring, K. Kutluer, J. Cohen, M, Cristiani, M. Mazzera, P. M Ledingham, and H. de Riedmatten. *New J. Phys.*, **16**, 113021 (2014).
[14] D. G England, P. S. Michelberger, T. F. M. Champion, K. F. Reim, K. C. Lee, M. R. Sprague, X.-M. Jin, N. K. Langford, W. S. Kolthammer, J. Nunn, and I. A. Walmsley. *J. Phys. B*, **45**, 24008 (2012).
[15] C. Clausen, F. Bussières, M. Afzelius, and N. Gisin. *Phys. Rev. Lett.*, **108**, 190503 (2012).
[16] M. Gündoğan, P. M. Ledingham, A. Almasi, M. Cristiani, and H. de Riedmatten. *Phys. Rev. Lett.*, **108**, 190504 (2012).
[17] Z.-Q. Zhou, W.-B. Lin, M. Yang, C.-F. Li, and G.-C. Guo. *Phys. Rev. Lett.*, **108**, 190505 (2012).
[18] E. Saglamyurek, J. Jin, V. B. Verma, M. D. Shaw, F. Marsili, S. W. Nam, D. Oblak, and W. Tittel. *Nature Photon.*, **9**, 83–87 (2015).
[19] M. Afzelius, C. Simon, H. de Riedmatten, and N. Gisin. *Phys. Rev. A*, **79**, 052329 (2009).
[20] F. Marsili, V. B. Verma, J. A. Stern, S. Harrington, A. E. Lita, T. Gerrits, I. Vayshenker, B. Baek, M. D. Shaw,

R. P. Mirin, and S. W. Nam. *Nature Photon.*, **7**, 210–214 (2013).

[21] P. C. Becker, N. A. Olsson, and J. R. Simpson. *Erbium-Doped Fiber Amplifiers - Fundamentals and Technology.* Academic Press, 1999.

[22] M. Bashkansky, I. Vurgaftman, A. C. R. Pipino, and J. Reintjes. *Phys. Rev. A* **90**, 053825 (2014)

[23] J. B. Altepeter, E. R. Jeffrey, and P. G. Kwiat. *Adv. At., Mol., Opt. Phys.*, **52**, 105–159 (2005).

[24] E. Saglamyurek, T. Lutz, L. Veissier, M. P. Hedges, C. W. Thiel, R. L. Cone and W. Tittel. arXiv:1507.03012 (2015).

[25] J. Nunn, N. K. Langford, W. S. Kolthammer, T. F. M. Champion, M. R. Sprague, P. S. Michelberger, X.-M. Jin, D. G. England, and I. A. Walmsley. *Phys. Rev. Lett.*, **110**, 133601 (2013).

[26] E. Saglamyurek, N. Sinclair, J. A. Slater, K. Heshami, D. Oblak, and W. Tittel. *New J. Phys.*, **16**, 065019 (2014).

[27] C. O'Brien, N. Lauk, S. Blum, G. Morigi, and M. Fleischhauer. *Phy., Rev. Lett.*, **113**, 063603 (2014).

[28] N. Sinclair, E. Saglamyurek, H. Mallahzadeh, J. A. Slater, M. George, R. Ricken, M. P. Hedges, D. Oblak, C. Simon, W. Sohler, and W. Tittel. *Phys. Rev. Lett.*, **113**, 053603 (2014).